ELSEVIER

Remarkably different structures and reaction mechanisms of ketoreductases for the opposite stereochemical control in the biosynthesis of BIQ antibiotics

Takaaki Taguchi,[a] Kanako Kunieda,[a] Mayuko Takeda-Shitaka,[b] Daisuke Takaya,[b] Noriaki Kawano,[a] Meriel R. Kimberley,[c] Kevin I. Booker-Milburn,[c] G. Richard Stephenson,[d] Hideaki Umeyama,[b] Yutaka Ebizuka[a] and Koji Ichinose[a,*]

[a]*Graduate School of Pharmaceutical Sciences, The University of Tokyo, Hongo, Bunkyo-ku, Tokyo 113-0033, Japan*
[b]*School of Pharmaceutical Sciences, Kitasato University, 5-9-1 Shirokane, Minato-Ku, Tokyo 108-8641, Japan*
[c]*School of Chemistry, University of Bristol, Cantock's Close, Bristol BS81TS, UK*
[d]*Wolfson Materials and Catalysis Centre, School of Chemical Sciences and Pharmacy, University of East Anglia, Norwich NR4 7TJ, UK*

Abstract—Two ketoreductases, RED1 and RED2, are involved in the biosynthesis of actinorhodin in *Streptomyces coelicolor* A3(2) and dihydrogranaticin in *S. violaceoruber* Tü22, respectively. They are responsible for the stereospecific reductions of the bicyclic intermediate to give (*S*)- or (*R*)-DNPA, although there is no similarity between their amino acid sequences. Biotransformation using synthetic analogous substrates revealed that the substrate specificities are quite different. Homology modelling studies and site directed mutagenesis showed remarkable differences in three-dimensional structures and catalytic mechanisms between RED1 and RED2.

1. Introduction

Benzoisochromanequinone (BIQ) antibiotics are members of a class of aromatic polyketides produced by streptomycetes. Actinorhodin (ACT, Fig. 1, **1**), produced by one of the most genetically characterized examples, *Streptomyces coelicolor* A3(2),[1] is a member of this group. The other related antibiotics include medermycin, frenolicin B, nanaomycin A (NNM), dihydrogranaticin A (DHGRA, Fig. 1, **2**), and griseusin B.[2] The stereochemistry at C-3 and C-15 allows the compounds to be further classified into either the ACT type, possessing the (3*S*,15*R*) configuration, or the NNM type with the opposite (3*R*,15*S*) configuration. Generally, the

* Corresponding author at present address: Research Institute of Pharmaceutical Sciences, Musashino University, Shinmachi, Nishi-tokyo-shi, Tokyo 202-8585, Japan. Tel./fax: +81 424 68 9184; e-mail addresses: ichinose@musashino-u.ac.jp; ichinose@mol.f.u-tokyo.ac.jp

stereochemistry of a functional group greatly influences its biological activity, therefore it is one of the most important medicinal issues to understand how the stereochemistry is determined as a step towards metabolic engineering to generate novel pharmacophores.

The biosynthetic gene clusters of ACT and DHGRA (the *act* cluster and the *gra* cluster) were sequenced.[3–9] We recently reported the full sequence of the medermycin biosynthetic gene cluster (the *med* cluster),[10] presenting the complete sequence information available on the three BIQ clusters. ACT and medermycin belong to the ACT type, and the other hand, DHGRA belongs to the NNM type. It is of great interest to make comparative analysis on these gene clusters to understand the biosynthesis and the mechanism of controlling the stereochemistry.

In the ACT biosynthesis, the C-3 absolute configuration is determined by stereospecific ketoreductase, RED1 encoded by *act* VI-ORF1.[11–13] RED1 recognizes the bicyclic intermediate (Fig. 1, **5**) as its substrate and reduces the prochiral C-3 keto-group. Subsequent
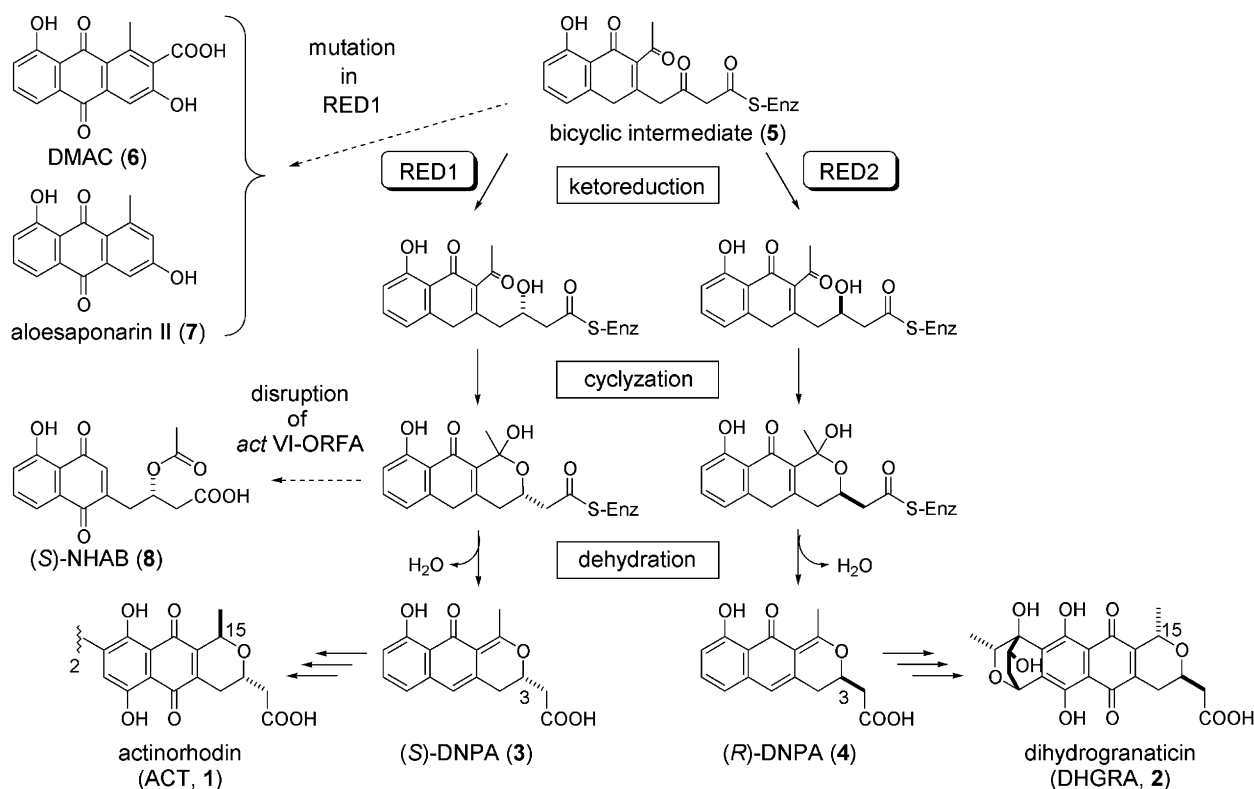
Figure 1. Proposed biosynthetic pathways of actinorhodin and dihydrogranaticin. The bicyclic intermediate produced by early steps enzymes is subjected to stereospecific ketoreductions by RED1/2. Subsequent cyclization and dehydration provide either (S)- or (R)-DNPA. Mutation of RED1 leads to production of the shunt products, DMAC/aloesaponarin II and disruption of *act* VI-ORFA leads to accumulation of the other shunt product, (S)-NHAB. The intermediates before (S)- or (R)-DNPA are tentatively shown as enzyme bound (*CO-S-Enz.*). Numbering of carbon atoms is based on the biosynthetic origin.

cyclization and dehydration produce the intermediate, 4-dihydro-9-hydroxy-1-methyl-10-oxo-3-*H*-naphtho-[2,3-*c*]-pyran-3-(S)-acetic acid, (S)-DNPA (Fig. 1, **3**). The bicyclic intermediate is produced by the enzymes of the early steps, consisting of β-ketosynthase (KS), chain length factor (CLF), acyl carrier protein (ACP), ketoreductase (KR), aromatase (ARO) and cyclase (CYC). In the *gra* cluster, the homologous genes encoding early steps enzymes are all present, and it is likely that the bicyclic intermediate is also produced in the DHGRA biosynthesis. We had assumed the presence of RED2 to reduce the bicyclic intermediate stereospecifically to give the intermediate (R)-DNPA (Fig. 1, **4**), and an obvious expectation was that RED2 is encoded by the homologue of *act* VI-ORF1. However, no RED1 homologue was found in the *gra* cluster. We found that *gra*-ORF5 and -ORF6 are candidates coding a reductase based on their nucleotide binding motifs as well as their similarity to the functionally related proteins, and have demonstrated that the *gra*-ORF6 product is essential for the production of (R)-DNPA,[14,15] suggesting its role as RED2.

Although RED1 and RED2 reduce the C-3 keto-group of the bicyclic intermediate and give (S)- or (R)-DNPA, BLAST 2 Sequences[16] showed no homology of the amino acid sequences between both enzymes.[15] Position-specific iterated BLAST (PSI-BLAST)[17] suggested that

RED1 is categorized into 3-hydroxyacyl-CoA dehydrogenase (3HAD) and RED2 into short-chain dehydrogenase/reductase (SDR). To clarify and compare the stereospecific reduction mechanisms, we have now investigated further the biochemistry and bioinformatics of RED1 and RED2.

2. Results

2.1. Biotransformation of synthetic analogous compounds

For the functional analysis of *gra*-ORF6, we had constructed plasmids based on an expression vector, pRM5.[18] This vector carries the genes of *act* I-ORF1 (KS), *act* I-ORF2 (CLF), *act* I-ORF3 (ACP), *act* III (KR), *act* VII (ARO), *act* IV (CYC) and *act* II-ORF4 (*Streptomyces* antibiotic regulatory protein, SARP). When introduced into the *act* cluster deficient mutant, *S. coelicolor* CH999, this vector gives rise to the production of the bicyclic intermediate in this transformant, but this compound cyclizes spontaneously to give the two shunt products, 3,8-dihydro-1-methoxyanthraquinone-2-carboxylic acid (DMAC) and aloesaponarin II[18] (Fig. 1 **6** and **7**). Addition of *act* VI-ORF1, encoding RED1, to pRM5 leads to construction of pIJ5660 and addition of *gra*-ORF6 encoding RED2 leads to pIK187. In the transformants carrying pIJ5660 or

pIK187, RED1 or RED2 recognized the bicyclic intermediate produced by early steps enzymes to give (S)- or (R)-DNPA.

As demonstrated previously,[19] the four analogous compounds were synthesized in place of the unstable bicyclic intermediate, and fed to the *S. coelicolor* CH999 transformant carrying pIJ5675, which is deficient in *act* I-ORF1 (KS) from pIJ5660. Deletion of KS gene causes no production of any ACT-related polyketides, but ACT biosynthetic enzymes except KS were expressed in this transformant. All the analogous compounds were enantioselectively reduced with the ACT-type configuration. Similarly, pIK196 was constructed by the deletion of *act* I-ORF1 from pIK190[15] for the reduction with (R)-configuration. The monocyclic and bicyclic analogous compounds were fed to the transformant carrying pIK196. RED2 turned out to give no reduction of these analogous compounds (Fig. 2). This result suggests that

substrate specificities are greatly different between RED1 and RED2, although both enzymes possibly recognize the same substrate motif.

2.2. Key catalytic residues of RED1 and RED2

Homology searches against the Protein Data Bank (PDB)[20] for RED1 and RED2 sequences using PSI-BLAST were carried out. In the case of RED1, L-3-hydroxyacyl-CoA dehydrogenase (3HAD) from human heart was found[21–23] as a homologous protein. This enzyme is essential to β-oxidation of fatty acids and catalyzes the dehydration of L-3-hydroxyacyl-CoA (Fig. 3), whose partial structure is similar to the reactive portion of the bicyclic intermediate. There are 43% similarity (identity + homology) between RED1 and 3HAD. In 3HAD, His158 and Glu170 were proved to be essential for activity by site directed mutagenesis and X-ray crystallography.[22,23] Alignment of the amino acid sequences
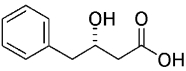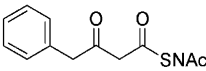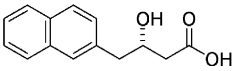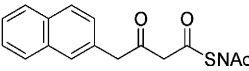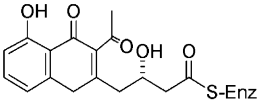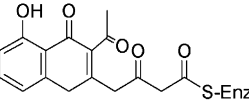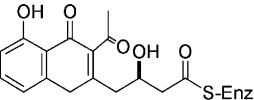

Figure 2. Results of biotransformation using synthetic analogous substrates. Left column shows the results of RED1, middle column shows the substrates, and right column shows the results of RED2. Bottom low shows the intact substrate and products of RED1/2, respectively, for comparison with analogous substrates.
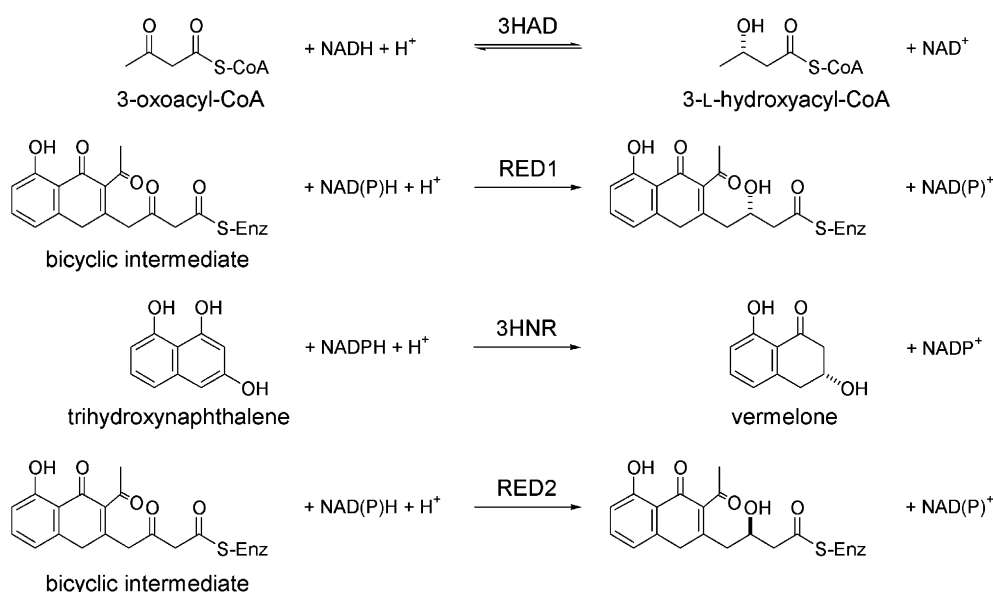
Figure 3. Comparison of reactions catalyzed by 3HAD, RED1, 3HNR and RED2 (the stereochemistry of vermelone is a proposal).

A

```
3HAD 151 QDRFAGLHFF NPVPVMKLVE VIKTPMT 177
RED1 122 PGRLVVAHPF NPPHIVPLVE VVRGERT 148
```

B

```
3HNR 161 LMGSITGQAK AVPKHAVYSG SKGAIET 187
RED2 141 NVSSIAG-SR PAGSSIPYAV SKAAIEH 166
TRII 143 FISSISG-AS ALPYEAVYGA TKGAMDQ 168
```

Figure 4. Alignment of the amino acid sequences between RED1 and 3HAD (A), and between RED2, 3HNR and TR-II (B). Bold characters show the conserved residues including the proposed key catalytic ones with underlines. The numbers indicate amino acid positions of each entry.

of RED1 and 3HAD showed that His129 and Glu141 in RED1 are well conserved and suggested that these two residues are essential for the reducing activity of RED1 (Fig. 4A). In the case of RED2, trihydroxynaphthalene reductase (3HNR) from *Magnaporthe grisea*[24] was found as a homologous protein. This enzyme catalyzes the reduction of trihydroxynaphthalene to afford vermelone in the melanin biosynthesis (Fig. 3). RED2 resembles 3HNR with 45% similarity. 3HNR is a typical SDR enzyme. Another SDR example, tropinone reductase II,[25] was also found. These enzymes have three key residues, Ser, Tyr and Lys as shown in Figure 4B, and the three residues are called as a catalytic triad (see Section 3). However, in the original sequence[7] of the *gra*-ORF6 protein, the third residue, Lys was substituted for Asn. The genomic fragment containing *gra*-ORF6, separately isolated from the rest of the *gra* cluster,[8] was examined to reveal that *gra*-ORF6 does indeed encode Lys (see Section 5). The catalytic triad was also conserved in RED2, and probably these residues should be essential for RED2 activity.

To test the importance of His129 and Glu141 in RED1, site directed mutagenesis was carried out. The strategy was based on the evaluation of (*S*)-DNPA production using CH999/pIJ5660.[12] Our approach was to introduce a His-tag, epitope sequence for Anti-Xpress™–Antibody–HRP (Invitrogen) and enterokinase cleavage site at N-terminal of RED1, allowing recombinant RED1 to be detected and isolated by Nickel-affinity column. The constructed plasmids were introduced into *S. coelicolor* CH999 followed by cultivation in liquid medium. The amounts of (*S*)-DNPA accumulated in culture medium were analyzed by HPLC. The modified version of pIJ5660, pIK572 (wild type: WT), gave comparable production of (*S*)-DNPA in its CH999 transformant. Subsequently, His129 was substituted with Ala (pIK573), Phe (pIK574) or Tyr (pIK575), and Glu141 was substituted with Ala (pIK576), Asp (pIK577) or Gln (pIK578). The productivities of (*S*)-DNPA of the transformants carrying the plasmids are summarized in Figure 5A. Only E141D mutant produced 1.1% amount of (*S*)-DNPA, and the other mutants produce no (*S*)-DNPA at all. This result shows that His129 is essential to RED1 activity. The difference between Glu and Asp is the length of side chain, which is likely to influence the reduction activity of RED1.
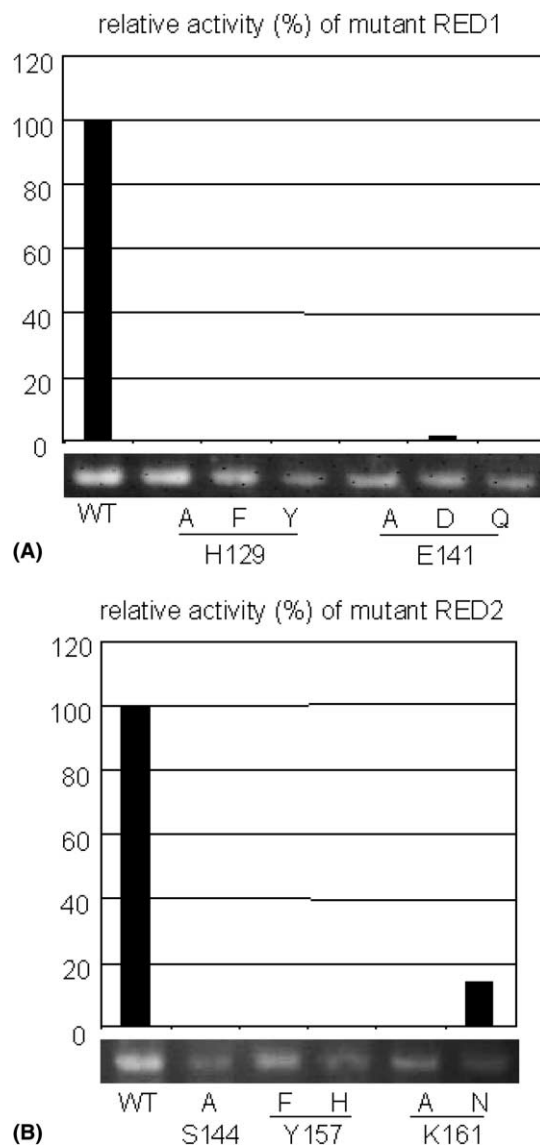
Figure 5. Summary of site directed mutagenesis of RED1 (A) and RED2 (B). Bar graphs illustrate the relative activities of mutant RED1/2s and photos shows the results of RT-PCR.

To investigate the role of Ser144, Tyr157 and Lys161, in RED2 site directed mutagenesis was performed in a similar manner to that for RED1. Plasmids were designed based on the plasmid, pIK187,[15] where *act* VI-ORF1 was replaced with an expression cassette of *gra*-ORF6. For these experiments, WT (pIK559), S144A (pIK560), Y157F (pIK561), Y157H (pIK562), K161A (pIK563) and K161N (pIK564) were constructed. Transformation and liquid culture were operated as for RED1, and amounts of (*R*)-DNPA in the culture medium were measured by HPLC. Results are shown in Figure 5B. S144A, T157F, T157H and K161A completely lost the reduction activity, while only K161N retained 16% activity.

2.3. Homology modelling of RED1 and RED2

To gain further insight, we constructed homodimer models of RED1–NAD$^+$ and RED2-NADPH com-

plexes using FAMS Ligand&Complex,[39] a fully automated modelling system for protein–protein complex including ligand. FAMS Ligand&Complex was developed by improving the procedures of FAMS,[26] a fully automated modelling system for monomer protein. The accuracy of FAMS Ligand&Complex has been demonstrated by an excellent example.[27] The high ability of FAMS Ligand&Complex, and also FAMS,[28] are mainly derived from the optimization protocol based on iterative cycles of side chain and main chain optimization. This protocol enables the conservation of the side chain torsional angles and main chain conformation within homologous proteins. After modelling, the quality of the stereochemistry of the models was checked. In each model structure, no unfavourable contacts between the atoms and no unnatural chiral centres were observed, and there were no bad steric clashes that prevented close interaction of the two monomers in the dimer. In the Ramachandran plot of the main chain $\phi - \varphi$ angles made by the program PROCHECK,[29] almost all of the non-glycine residues were in the most favoured or allowed regions. All the ω angles were trans-planar.

In the case of RED1, we constructed a homodimer model using 3HAD as the reference protein (Fig. 6A), because the structure of 3HAD suggested that RED1 exists as a dimer. Although the sequence identity between RED1 and 3HAD is only 24%, the low E-value (1×10^{-117}) obtained by PSI-BLAST indicates that RED1 has a similar fold to 3HAD and that 3HAD could be used as the reference protein for RED1. Moreover, the amino acid residues in the active site region are highly conserved between RED1 and 3HAD, which indicates that the alignment of the active site region is reliable and that the active site structure of RED1
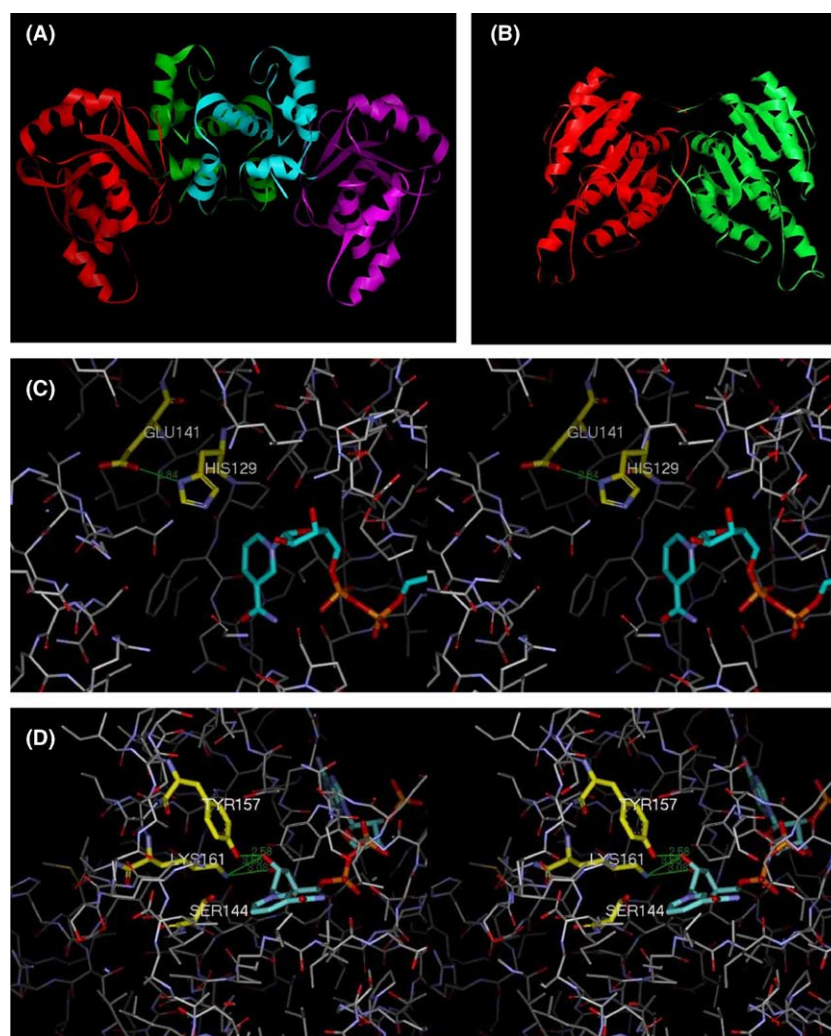
Figure 6. Model structures of RED1 and RED2. (A) Homodimer model of RED1. In one subunit, N-terminal and C-terminal domains are shown in red and green, respectively. In the other subunit, N-terminal and C-terminal domains are shown in magenta and cyan, respectively. (B) Homodimer model of RED2. Two subunits are shown in red and green. (C) Stereoview of the active site region of RED1 model. Oxygen, nitrogen and phosphorus atoms are coloured in red, blue and orange, respectively. Carbon atoms of His129 and Glu141 are coloured in yellow and those of NAD$^+$ are coloured in cyan. Hydrogen bonds are indicated with green lines. (D) Stereoview of the active site region of RED2 model. Oxygen, nitrogen and phosphorus atoms are coloured as (C). Carbon atoms of Ser144, Tyr157 and Lys161 are coloured in yellow and those of NADPH are coloured in cyan. Hydrogen bonds are indicated with green lines. Models were visualized using a WEBLAB VIEWERLITE 4.0 (Molecular Simulations Inc.).

should be very similar to that of 3HAD. These factors suggested that the model structure is reliable especially in the active site region. In the PDB, 11 structures of 3HAD or mutant 3HAD were registered. One of them (PDB code: 1F0Y) is a complex with NAD^+ and acetoacetyl-CoA with the highest resolution, therefore we chose 1F0Y as the reference protein. Because the reference structure is the complex structure of 3HAD–NAD^+, we constructed RED1–NAD^+ complex model using FAMS Ligand&Complex. The model comprises residues 1–279 out of 307 amino acids. The N-terminal domain (Met1-Ala173) has Rossman fold, a common tertiary structure found in NAD(P)-binding proteins. The C-terminal domain (Ala179-Ala279) is involved in subunit dimerization. The two domains are connected by a short loop (Leu174-Ala178). In the active site region, Nδ1 atom of His129 is hydrogen bonded with Oε1 atom of Glu141 (Fig. 6C), as the corresponding atom pair hydrogen bonded in 3HAD.

In the case of RED2, we constructed a homodimer model using 3HNR as the reference protein (Fig. 6B), because the structure of 3HNR suggested that RED2 exists as a dimer. The sequence identity between RED2 and 3HNR is 32%, and *E*-value (4×10^{-59}) was low enough that 3HNR could be used as the reference protein for RED2. These indicate that the model structure is reliable. In the PDB, four structures were found for the 3HNR in complex with the combinations of NADPH and four inhibitors. Among them, we used an X-ray structure (PDB code: 1DOH) as the reference structure. The model consists of residues 3–248 out of 249 total amino acids. It has a single-domain structure with the Rossman fold to bind NAD(P)H. In the model, Nζ atom of Lys161 forms hydrogen bonds to 2′- and 3′-hydroxyl groups of ribose of NADPH, and Oη atom of Tyr157 forms a hydrogen bond to 2′-hydroxyl group of ribose of NADPH (Fig. 6D). The corresponding atom pairs also form hydrogen bonds in 3HNR. Tyr157 is perfectly located as a proton donor for a hemiketal formation of the reduced product. Lys161 appears to be placed to form possible hydrogen bond with ribose of NADPH.

2.4. Expression analysis

To evaluate the expression levels of mutants of RED1 and RED2, expression analysis was carried out. Transformants carrying wild type and mutant *act* VI-ORF1 or *gra*-ORF6 were cultivated under the same conditions as above. Protein preparations from mycelia of each transformant were used for analysis with SDS-PAGE and western blotting. Surprisingly, the bands corresponding to RED1 or RED2 were not detected even for the transformants carrying the plasmids of WT RED1 (pIK572) and RED2 (pIK559) genes. (Data not shown.) Therefore, we tried transcriptional analysis by reverse transcription (RT)-PCR. Total RNA extracted from frozen mycelia was used as the template for RT-PCR with the specific primers used. Expected PCR products were detected from all transformants (Fig. 5), demonstrating that mutation of *act* VI-ORF1 and *gra*-ORF6 had not abolished their transcriptions.

3. Discussion

3.1. Difference of substrate specificity

The biotransformation experiments suggest that the substrate specificities of RED1 and RED2 are different. An explanation for this might arise from the significant difference in the domain structures of both enzymes. 3HAD, the template of RED1, consists of N-terminal domain and C-terminal domain and L-3-hydroxyacyl-CoA as a substrate binds in the cleft between the two domains. The significant domain shift observed in the structures with and without ligands clearly suggested that the N-terminal domain rotates inward toward the C-terminal domain when the substrate binds.[22] A similar domain shift would occur in RED1, allowing the broader substrate specificity. On the other hand, RED2 is a single-domain protein unlikely to provide significant conformation change, implying the more strict substrate specificity.

PSI-BLAST showed that RED2 resembles 3-oxoacyl-ACP reductases/FabG from various bacteria. FabG is an essential component of type II fatty acid synthesis and catalyzes the reduction of C-3 keto-group of 3-oxoacyl-ACP in bacteria. Especially FabG from *Escherichia coli* was shown to bind ACP for the reduction.[30,31] This might explain the reason why RED2 is unable to reduce analogous compounds. Possibly, for the reduction by RED2, the bicyclic intermediate and analogous substrates have to be bound to ACP.

3.2. Proposed mechanism of the reduction by RED1

The structural study of 3HAD suggested Glu170 to be appropriately interacted with His158 in such a way that the pK_a of His158 is elevated.[23] This suggestion and all of the present data led us propose the reaction mechanism of RED1 as shown in Figure 7A. His129 is activated by Glu141 and proton of the His129 side chain is used to reduce of the C-3 keto-group. Additionally, taking account into the mechanism of 3HAD, *pro-S* proton of nicotinamide ring of NAD(P)H would be transferred to C-3 of the bicyclic intermediate. Because in H129A and H129F mutants Ala and Phe had no transferable protons, they showed no activity. The lack of reducing activity observed for the H129Y mutant is explained by the rather basic property of the hydroxyl moiety of Tyr, rendering it incapable of functioning as a proton donor.

In 3HAD, substitution of Glu170 with Gln retained the function but with a resulting 30-fold reduction in activity. We expected that E141Q mutant would also show lower activity, but this mutant has no activity. Possibly the role of Glu141 would be more important in RED1 than in 3HAD. Interestingly, E141D mutant showed very low activity. By substitution of Glu with Asp, side chain became shorter, but a weak hydrogen bond could form to allow His129 to be activated. These results well agree with the proposed mechanism of RED1 (Fig. 7A).
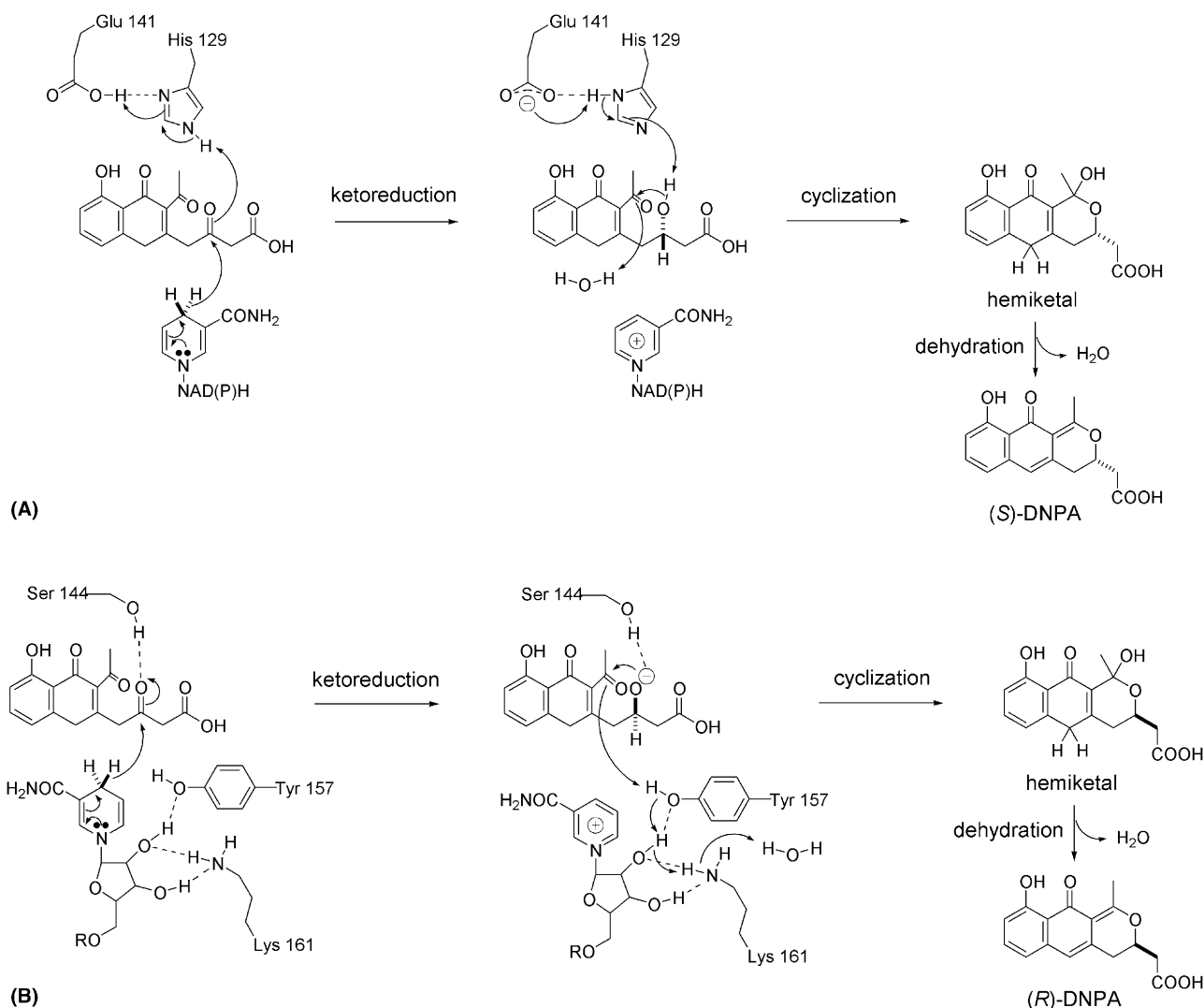
Figure 7. Proposed mechanisms of the reactions catalyzed by RED1 (A) and RED2 (B), ketoreduction and cyclization and subsequent dehydration to afford either (S)-DNPA or (R)-DNPA.

3.3. Proposed mechanism of the reduction by RED2

As mentioned previously,[15] RED2 belongs to the SDR family. Highly conserved Ser-Tyr-Lys residues (catalytic triad) are involved in SDR catalysis, where the Tyr residue functions as a catalytic acid–base for proton transfer together with the Ser residue interacting the reactive oxygen of a substrate.[25] Indeed, the pK_a values attributable to the triad Tyr was experimentally estimated to 7.5 for a *Dorosophila* alcohol dehydrogenase.[32] Crystallographic studies[24,25] showed that the triad Lys residue is hydrogen bonded to both the 2′- and 3′-hydroxyl groups of the nicotinamide ribose of a cofactor likely to contribute to the acid–base catalysis. This is a clear distinction from our study on RED1 that the mutant (H129Y) is catalytically inactive, indicating the Tyr residue incapable of acting as a proton donor. In the RED2–NADPH complex model, Nζ atom of Lys161 is hydrogen bonded to both 2′- and 3′-hydroxyl groups of NADPH, and Oη atom of Tyr157 is hydrogen bonded to 2′-hydroxyl group of ribose of NADPH (Fig. 6D). Based on the results of site directed muta-

genesis and modelling of the complex, we proposed the reaction mechanism of RED2 as shown in Figure 7B.

In the proposed mechanism of 3HNR, Ser164 of the catalytic triad only stabilizes the reactive keto-group, but S144A mutant of RED2 lost its activity. This might suggest that the hydrogen bond between the proton of Ser144 side chain and the oxygen atom of C-3 keto-group is critical in RED2. In 3HNR and TR-II *pro-S* proton of nicotinamide ring of NADPH was transferred to substrates. It is likely that in RED2 *pro-S* proton of nicotinamide ring of NADPH was used to give (R) configuration at C-3. The model of RED2 in complex with NADPH supports this possibility. Substitution of Tyr157 to Phe157 might not change the three-dimensional structure of mutant RED2, but the lack of the hydroxy moiety must destroy the salt bridge between NAD(P)H, Tyr and Lys, so causing the loss of activity. Similarly, in Y157H, the salt bridge could not be formed because the pK_a and structure of side chain of Tyr and His are greatly different. It is reasonable that Y157F and Y157H mutants showed no activity. Probably the

destruction of salt bridge occurred in the K161A mutant but K161N might be slightly different. The structures of the side chains, Lys161 and Asn, both possess an amino moiety. It is possible that Asn161 in K161N mutant formed weak hydrogen bond with hydroxyl moiety of ribose of NAD(P)H to form incomplete salt bridge and then showed weak activity.

3.4. Possibility of cyclization after ketoreduction

The chemically spontaneous hemiketal formation of the 3-keto reduced products could also be catalyzed in an enzyme cavity. We propose here a catalytic cyclization in RED1/RED2 (Fig. 7). The hydroxyl group would be reactivated by His129 to attack the C-15 keto-group to initiate cyclization to regenerate the active amino acid residues (Glu141 and His129) in favour of a unidirectional biosynthetic pathway to ACT (Fig. 7A). Similarly, the C-15 keto-group in RED2 catalysis could be located close to the Tyr157 residue. Because the Ser residue is shown to stabilize substrate binding by hydrogen bonding to the reactive oxygen, it is likely that an anionic oxygen of C-3 is involved in the cyclization followed by the proton abstraction from Tyr157 (Fig. 7B).

The production of (S)- or (R)-DNPA by co-expression of RED1/2 with the early biosynthetic enzymes in S. coelicolor CH999 indicates an efficient cyclization and dehydration after the ketoreduction of the bicyclic intermediate in the recombinant systems (Fig. 7). It would be interesting to know if the dehydration also proceeds in the RED1/RED2 cavity. In the case of S. coelicolor, we reported that act VI-ORFA disruptant of S. coelicolor accumulated not only (S)-DNPA but also the novel shunt product, 1,4-naphthoquinone-8-hydroxy-3-[(3S)-acetoxybutyric acid], (S)-NHAB (Fig. 1, 8).[33,34] Interestingly, it also produces a reduced amount of ACT compared with the wild type strain. The structure of (S)-NHAB indicates that disruption of act VI-ORFA causes to decrease the efficiency of dehydration from a hemiketal. Database search indicated that a family of act VI-ORFA genes is widely distributed in the gene clusters for Streptomyces aromatic polyketides including non-BIQ metabolites[34] exclusively with carbocyclic rings. The combined data makes us favour an idea of more regulatory role of this gene family. We are undertaking its biochemical characterization such as coexpression with the relevant act biosynthetic enzymes. Taken together, the RED1 catalytic process appears to be responsible for the steps of dehydration as well as 3-keto reduction (Fig. 7), and act VI-ORFA seems to increase the efficiency of dehydration.

3.5. Comparison between RED1 and RED2

The present study using homology modelling and mutagenesis showed the marked difference in the structure and possible catalytic mechanism of RED1 and RED2. Suppose two enzymes with the opposite stereochemistries recognize a common substrate, one could expect significant sequence similarity between the two enzymes, at least for the substrate recognition. Tropinone reductase I and II (TR-I and TR-II) from plant,

Hyoscyamus niger, are such examples. The two enzymes belonging to SDR are involved in the biosynthesis of tropane alkaloid and recognize tropinone as substrate to give tropine (3α-hydroxytropane) and pseudotropine (3β-hydroxytropane), respectively.[25] But TR-I and TR-II share 64% of the same amino acid residues and conserve overall structures. While the two enzymes exist in the same plant, RED1 and RED2 are from different bacterial strains, indicating RED1 and RED2 to be evolved from different origins. One possibility of origin of RED1 is 3-hydroxyacyl-CoA dehydrogenase (3HAD), which is involved in β-oxidation of fatty acid in the primary metabolism. It is possible that one of the copies of 3HAD was transferred from the other location of genome to the act cluster with mutation and gained the reduction activity of the bicyclic intermediate. Indeed, there are nine homologues of 3HAD in the S. coelicolor genome, whose complete genome sequence available.[1] On the other hand, a large number of RED2 homologues are found in various bacteria. It is intriguing to assume that the gra-ORF6 gene, encoding RED2, could have been duplicated from its flanking gra-ORF5, which encodes KR, followed by further evolution to gain 3-keto reducing activity.

4. Conclusion

An increasing number of biosynthetic gene clusters responsible for secondary metabolites including antibiotics have been cloned and sequenced. However, for the purpose of metabolic engineering to produce unnatural compounds towards effective therapeutics, we ultimately have to understand the catalytic mechanisms for each biosynthetic enzyme. One of the most important key enzymes is concerned with the stereochemical control of a target compound. We clarified here novel examples, RED1 and RED2. Actually the two enzymes catalyze the ketoreduction at C-3 of the bicyclic intermediate to give (S)- or (R)-DNPA, about various aspects, like amino acid sequences, predicted three-dimensional structures, the substrate specificity, and reduction mechanism, RED1 and RED2 were shown to be dissimilar. This suggests that it is not simple to know how to control stereochemistry in combinatorial biosynthesis and we have to approach to clarify the characteristics of each biosynthetic enzyme from various aspects. X-ray crystallographic and NMR studies give us much information on the three-dimensional structure of a protein of interest, but still to a limited extent. Homology modelling of a target protein is a complementary and useful method to predict protein structures and their putative functions. The present study demonstrated a successful example of a functional genomics approach based on bioinformatics and biochemistry.

5. Experimental procedures

5.1. Bacterial strains and DNA manipulation

The host strain for all the plasmids was S. coelicolor A3(2) CH999,[18] which is an act cluster deficient strain

(*proA1*, *argA1*, *SCP1⁻*, *SCP2⁻*, *redE60*, *Δact*). General DNA manipulations for transformation were according to standard procedures.[35] Streptomyces manipulations were as described.[36]

5.2. Plasmid for biotransformation

Deletion of *Pac*I–*Nsi*I fragment from pIK190[15] followed by Klenow treatment gave pIK196.

5.3. PCR and sequence analysis

All PCR was carried out using RoboCyler® Gradient40 (Stratagene) with *Ex-Taq* DNA polymerase (TaKaRa). PCR programme except site directed mutagenesis was as follows: 94 °C, 5 min; [94 °C, 1 min; 70 °C, 30 s; 72 °C, 1 min] × 25 cycles; 72 °C, 10 min. PCR programme for site directed mutagenesis was as follows: 95 °C, 10 min; [95 °C, 1 min; 56 °C, 30 s; 72 °C, 1 min] × 25 cycles; 72 °C, 10 min. Sequence analysis was performed on automated DNA sequencers, model 4000L (LI-COR) and PRISM-3100 (ABI).

5.4. Sequence analysis of *gra*-ORF6

A plasmid pIK109[14] derived from the pBluescript SK(−) based subclone (B8) carrying the *Bam*HI fragment of the *gra* cluster[8] was used for sequence analysis. Previously reported sequence,[7] '469 AGCAA*T*GGC-GGCCATCGAGCACAGACT 505' was corrected to the revised one, '469 AGCAAGGCGGCCATCGAG-CACA*T*GACT 505'. The changes of thymine (shown in bold italic) changed the amino acid sequence from '160 S**N**GGH**R**AQT 168' to '160 S**K**AAIE**H**MT 168' (the residues relevant to catalytic triad are shown in bold).

5.5. Plasmids for site directed mutagenesis of RED2

To construct plasmids for site directed mutagenesis, *gra*-ORF6 was amplified from pIK110[14] with the sense primer, 5′-GGA*AGATCT*A**TG**GCCACCGACGCGC-CCGA-3′ (italic shows *Bgl*II site and bold start codon), and the antisense primer, 5′-CCG*GAATTC*AG-GGGGCGGG**TCA**GAGGAGGT-3′ (italic, *Eco*RI site; bold, stop codon). PCR products were digested by *Eco*RI and *Bgl*II and ligated to pRSET B (Invitrogen) to give pIK403. To engineer the nucleic acid sequence corresponding to His-tag, epitope of Antibody and enterokinase cleavage site, three-step PCR was carried out from pIK403. N-terminal 300 bp region of *gra*-ORF6 was engineered as follows: 5′-*GAATTC*G-CATGC**GGAGG**GATATACATATGCGGGGCTCC-CATCATCATCATCATCAC**GAGCTGTACGACGAC-GACGACAAG**GATCCGAGCTCG*AGATCT*A**TG**GC-CACCGAC-3′ (italic, *Eco*RI site; underline, *Sph*I site; bold, ribosomal binding site; second underline, His x6-tag; second bold, epitope for Anti-Xpress™–Antibody–HRP; bold and underline, enterokinase cleavate site; second italic *Bgl*II site; third bold, start codon of *gra*-ORF6). This PCR product was subcloned into pT7Blue vector (Novagen) to give pIK532. To construct C-terminal 450 bp region of *gra*-ORF6, five antisense primers,

5′-CCCGCGAT**GGC**CGACACGTT-3′ (S144A), 5′-CT-CACCGC**GAA**AGGGATCGA-3′ (Y157F), 5′-CTCA-CCGC**GTG**AGGGATCGA-3′ (Y157H), 5′-TCGATG-GCCGC**GGC**GCTCAC-3′ (K161A), 5′-TCGATGG-CCGC**GTT**GCTCAC-3′ (K161N) and the sense primer, 5′-ACCTG**GCGGCCGC**CACCCCC-3′ (underline, *Not*I site), were used for PCR, and then each PCR product and antisense primer 5′-AAGCTT-*GCA*-*TGC*GGGCGGG**TCA**GAGGAGGT-3′ (underline, *Hind*III site; italic, *Sph*I site; bold, stop codon) were used for second PCR. PCR fragments (450 bp) were subcloned into T7blue vector to give pIK351–pIK355. Combination of *Not*I–*Hind*III fragments of 450 bp from pIK179 and pIK351–pIK355 with engineered N-terminal region on pIK532 lead to construction of *Sph*I cassettes of engineered *gra*-ORF6 on pIK540–pIK545. Each *Sph*I cassette was subcloned to pIJ5654 to give pIK553–pIK558, and then *Xba*I–*Eco*RI fragment of 5.5 kbp was digested and substituted into pRM5 to construct pIK559–pIK564 finally.

5.6. Plasmids for site directed mutagenesis of RED1

To construct plasmids for site directed mutagenesis of RED1, *act* VI-ORF1 was amplified by PCR from pIJ5660 with the sense primer, 5′-GGA*AGATCT*A**TG**-AGCACCGTGACAGTGATCG-3 (italic, *Bgl*II site; bold, start codon), and the antisense primer, 5′-CCG-*GAATTC*TC**ACT**TGGTCTCCTCCTGGGG-3′ (italic, *Eco*RI site; bold, stop codon). PCR product was digested by *Eco*RI and *Bgl*II and ligated to pRSET B to give pIK402 (*act* VI-ORF1). Using pIK402 as a template, sense primer, 5′-CGG*CTGCAG*T-CGGCGCTGCT-3′ (underline, *Pst*I site), and antisense primer, 5′-AAGCTT*GCATGC*GAATTCTC**ACT**TG-GTCTCCTCCT-3′ (first underline, *Hind*III site; italic, *Sph*I site; second underline, *Eco*RI; bold, stop codon), 380 bp fragment was amplified and subcloned into T7blue vector to give pIK517. A *Pst*I–*Hind*III region on pIK402 was substituted by the *Pst*I–*Hind*III fragment on pIK517 and pIK518 was constructed. To construct mutant *act* VI-ORF1, six antisense primers, 5′-TTGAACGGT**GC**CGCGACGAC-3′ (H129A), 5′-TT-GAACGGG**AA**CGCGACGAC-3′ (H129F), 5′-TTGA-ACGGG**TA**CGCGACGAC-3′ (H129Y), 5′-CGGAC-CAC**TGC**GACCAGCGG-3′ (E141A), 5′-CGGAC-CAC**ATC**GACCAGCGG-3′ (E141D), 5′-CGGAC-CAC**TTG**GACCAGCGG-3′ (E141Q) and the sense primer, 5′-AGAGATCGGA**GCGGCCGC**CC-3′ (underline, *Not*I site), were used for first PCR, and then each first PCR product and antisense primer 5′-TC**GAG-CTC**CTCGACGGTCAC-3′ (underline, *Sac*I site) were used for second PCR. *Not*I–*Sac*I region on pIK518 was substituted by 350 bp PCR products to give pIK520–pIK525. A *Bam*HI–*Hind*III fragments of pIK518 and pIK520–pIK525 were ligated to pIK532 and *Sph*I cassettes of *act* VI-ORF1 were constructed on pIK519 and pIK526—pIK531. Each *Sph*I cassette was subcloned to pIJ5654 to give pIK533–pIK539. After pIK533–539 was partially digested by *Eco*RI followed by Klenow treatment, *Xba*I–*Eco*RI fragment of 5.5 kbp was digested and substituted into pRM5 to construct pIK572–pIK578.

5.7. Culture

Seed cultures (10 mL) were grown as previously described.[33] Production cultures were modified as follows. Aliquots (5 mL) of the culture were inoculated to 50 mL of R4 medium consisting of glucose 1%, yeast extract (DIFCO) 0.1%, BACTO™ casamino acid 0.01%, K_2SO_4 0.02%, $MgCl_2 \cdot 6H_2O$ 1%, TES buffer 0.56%, trace element solution[36] 0.2% v/v, $CaCl_2 \cdot 2H_2O$ 0.4%, L-proline 0.3%, pH 7.2 in 500 mL Erlenmyer flasks, which were grown on a rotary shaker at 200 rpm, 28 °C. The term of cultures depended on each experiment.

5.8. HPLC analysis

Part of culture (1 mL) from each flask was transferred to centrifuge tube and centrifuged at 20,000g for 5 min. Supernatant (100 μL) was directly subjected to reversed-phase HPLC analysis on a TOSOH 8020 system under the following conditions: column, TSK gel ODS-80T_M (4.6 i.d. × 150 mm, TOSOH); column temperature, 40 °C; gradient elution, solvent A (0.5% AcOH in CH_3CN) and solvent B (0.5% AcOH in deionized H_2O), gradient profile depends on each experiment; flow rate, 1.0 mL/min; detection, absorption between 250–600 nm using photo-diode array detector (PD-8020, TOSOH).

5.9. Synthesis and biotransformation

Monocyclic and bicyclic analogous compound were synthesized as described.[19] Each compound was dissolved or suspended in MeOH with 50 mg/mL. Following strains were used for biotransformation, the host strain CH999 as negative control, transformant CH999/pIJ5674 as another negative control, CH999/pIJ5675 as positive control, and CH999/pIK196. Forty-eight hours after production culture started, 1 mL of solution was added to each flask and for further two days cultures were continued at the same condition. Supernatant of cultures were directly subjected to HPLC and analyzed under the following gradient profile: 0–20 min, 10–70% A; 20–23 min, 70–95% A; 23–27 min, 95% A; 27–30 min, 95–10%.

5.10. HPLC analysis for site directed mutagenesis

Production cultures were continued for 110 h (5 days). HPLC analysis was carried out with following gradient profile: 0–5 min, 35%; 5–20 min, 35–70%; 20–23 min, 70–95%; 23–27 min, 95%; 27–30 min, 95–35%.

5.11. Expression analysis of RED1 and RED2

Mycelia of each transformant collected by filtration were immediately frozen in liquid N_2 and stored at −30 °C before use. Frozen mycelia were ground on a mortar with a pestle together with ×0.5 w/w of Polyclar AT and ×1 w/w of aluminium oxide. Then added was ×5 v/w of extraction buffer consisting of 20 mM Tris–HCl (pH 7.8), 10 mM $MgCl_2$, 20 mM NH_4Cl, 1 mM dithiothreitol and Complete Mini, EDTA-free (Roche, one tablet in 10 mL buffer). Broken mycelia was suspended in extraction buffer and collected into a centrifugation tube. After centrifugation at 20,000g, 4 °C, for 10 min, supernatant was transferred to other fresh tube as crude extract. Crude extracts were applied on a 13% gel for SDS-PAGE with 10 μL/well and developed at 200 V for 45 min. Then proteins on the gel were blotted on nitrocellulose membrane by electroblotting at 100 V for 90 min. The blotted membranes were incubated in Tris–saline–buffer containing Anti-Xpress™–Antibody–HRP and then stained using Konica Immunostain kit.

5.12. RT-PCR

Frozen mycelia of each transformant (0.1–0.15 g) was ground on a mortar with a pestle and suspended in 1 mL of ISOGEN (Nipponegene). Extraction of RNA was followed by manufacture's manual and repeated twice. RNA was dissolved in purified water 50 μL, and concentration was measured by UV-spectroscopy. After 2 μg of RNA was treated with DNaseI (Invitrogen, Amp. Grade), reverse transcription (RT) was carried out with Thermoscript RT (Invitrogen) and specific primers for *act* VI-ORF1, 5′-GCTCCGATCTCT-GCGAACAA-3′ or *gra*-ORF6, 5′-GGCGTTGTTGA-CGAGGACGT-3′. PCR was carried out with *Ex-Taq* DNA polymerase using 1 μL of RT solution as template. Antisense primers were as same as the primers for RT. The sense primer, 5′-GGCTCCCATCATCATCAT-CAT-3′ was used for both genes. PCR fragments (the expected sizes, *act* VI-1: 350 bp; *gra*-ORF6: 320 bp) were analyzed on 2% agarose electrophoresis. As negative control, extraction of RNA from the frozen mycelia of *S. coelicolor* CH999 carrying pRM5 and RT-PCR was carried out under the same condition. No amplified products were detected.

5.13. Homology modelling of RED1–NAD$^+$ and RED2–NADPH complexes

Model structures of RED1–NAD$^+$ and RED2–NADPH complexes were constructed based on homology modelling methods. Searching for reference proteins and sequence alignments was performed using PSI-BLAST. The reference protein for RED1 was the X-ray structure of 3-L-hydroxyacyl-CoA dehydrogenase (3HAD) in complex with acetoacetyl-CoA and NAD$^+$ (PDB code: 1F0Y) and that for RED2 was the X-ray structure of trihydroxynaphthalene reductase (3HNR) in complex with NADPH and 4-nitroinden-1-one (PDB code: 1DOH). The sequence alignments produced by PSI-BLAST were manually adjusted taking biologically important regions and secondary structure into consideration using CHIMERA modelling system.[37,38] Then we constructed homodimer models of RED1–NAD$^+$ and RED2–NADPH complexes using the computer software FAMS Ligand&Complex based on the homodimer structures of 3HAD–NAD$^+$ and 3HNR–NADPH complexes, respectively. The molecular coordinates (PDB files) of the RED1 and RED1 are freely available upon request to the corresponding author.

6. Accession numbers

The modified DNA and deduced protein sequence of *gra*-ORF6 in this paper was deposited in the DDBJ, EMBL and GenBank nucleotide sequence databases under the accession number AB167818.

Acknowledgements

References and notes

1. Bentley, S. D.; Chater, K. F.; Cerdeno-Tarraga, A. M.; Challis, G. L.; Thomsom, N. R.; James, K. D.; Harris, D. E.; Quail, M. A.; Kieser, H.; Harper, D.; Bateman, A.; Brown, S.; Chandra, G.; Chen, C. W.; Collins, M.; Cronin, A.; Fraser, A.; Goble, A.; Hidalgo, J.; Homsby, T.; Howarth, S.; Huang, C. H.; Kieser, T.; Larke, L.; Murphy, L.; Oliver, K.; O'Neil, S.; Rabbinowitsch, E.; Rajandream, M. A.; Rutherford, K.; Rutter, S.; Seeger, K.; Saunders, D.; Sharp, S.; Squares, R.; Squares, S.; Taylor, K.; Warren, T.; Wietzorrek, A.; Woodward, J.; Barell, B. G.; Parkhill, J.; Hopwood, D. A. *Nature* **2002**, *417*, 141.
2. Hopwood, D. A. *Chem. Rev.* **1997**, *97*, 2465.
3. Fernandez-Moreno, M. A.; Caballero, J. L.; Hopwood, D. A.; Malpartida, F. *Cell* **1991**, *66*, 769.
4. Fernandez-Moreno, M. A.; Martinez, E.; Boto, L.; Hopwood, D. A.; Malpartida, F. *J. Biol. Chem.* **1992**, *267*, 19278.
5. Caballero, J. L.; Martinez, E.; Malpartida, F.; Hopwood, D. A. *Mol. Gen. Genet.* **1991**, *230*, 401.
6. Fernandez-Moreno, M. A.; Martinez, E.; Caballero, J. L.; Ichinose, K.; Hopwood, D. A.; Malpartida, F. *J. Biol. Chem.* **1994**, *269*, 24854.
7. Sharman, D. H.; Malpartida, F.; Bibb, M. J.; Kieser, H. M.; Bibb, M. J.; Hopwood, D. A. *EMBO J.* **1989**, *8*, 2717.
8. Bechthold, A.; Sohng, J. K.; Smith, T. M.; Chu, X.; Floss, H. G. *Mol. Gen. Genet.* **1995**, *248*, 610.
9. Ichinose, K.; Bedford, D. J.; Tornus, D.; Bechthold, A.; Bibb, M. J.; Revill, W. P.; Floss, H. G.; Hopwood, D. A. *Chem. Biol.* **1998**, *5*, 647.
10. Ichinose, K.; Ozawa, M.; Itou, K.; Kunieda, K.; Ebizuka, Y. *Microbiology* **2003**, *149*, 1633.
11. Ichinose, K.; Taguchi, T.; Ebizuka, Y.; Hopwood, D. A. *Acytinomycetologica* **1998**, *12*, 99.
12. Ichinose, K.; Surti, C.; Taguchi, T.; Malpartida, F.; Booker-Milburn, K. I.; Stephenson, G. R.; Ebizuka, Y.; Hopwood, D. A. *Bioorg. Med. Chem. Lett.* **1999**, *9*, 395.
13. Taguchi, T.; Itou, K.; Ebizuka, Y.; Malpartida, F.; Hopwood, D. A.; Surti, C. M.; Booker-Milburn, K. I.; Stephenson, G. R.; Ichinose, K. *J. Antibiot.* **2000**, *53*, 144.
14. Ichinose, K.; Taguchi, T.; Bedford, D. J.; Ebizuka, Y.; Hopwood, D. A. *J. Bacteriol.* **2001**, *183*, 3247.
15. Taguchi, T.; Ebizuka, Y.; Hopwood, D. A.; Ichinose, K. *J. Am. Chem. Soc.* **2001**, *123*, 11376.
16. Tatusova, T. A.; Madden, T. L. *FEMS Microbiol. Lett.* **1999**, *174*, 247.
17. Altchul, S. F.; Madden, T. L.; Schäffer, A. A.; Zhang, J.; Zhang, Z.; Miller, W.; Lipman, D. J. *Nucleic Acid Res.* **1997**, *25*, 3389–3402.
18. McDaniel, R.; Ebert-Khosla, S.; Hopwood, D. A.; Khosla, C. *Science* **1993**, *262*, 1546.
19. Anson, C. E.; Bibb, M. J.; Booker-Milburn, K. I.; Clissold, C.; Haley, P. J.; Hopwood, D. A.; Ichinose, K.; Revill, W. P.; Stephenson, G. R.; Surti, C. M. *Angew. Chem., Int. Ed.* **2000**, *39*, 224.
20. Berman, H. M.; Westbrook, J.; Feng, Z.; Gilliland, G.; Bhat, T. N.; Weissig, H.; Shindyalov, I. N.; Bourne, P. E. *Nucleic Acids Res.* **2000**, *28*, 235.
21. Barycki, J. J.; O'Brien, L. K.; Bratt, J. M.; Zhang, R.; Sanixhvili, R.; Strauss, A. W.; Banaszak, L. J. *Biochemistry* **1999**, *38*, 5786.
22. Barycki, J. J.; O'Brien, L. K.; Strauss, A. W.; Banaszak, L. J. *J. Biol. Chem.* **2000**, *275*, 27186.
23. Barycki, J. J.; O'Brien, L. K.; Strauss, A. W.; Banaszak, L. J. *J. Biol. Chem.* **2001**, *276*, 36718.
24. Liao, D.-I.; Basarab, G. S.; Gatenby, A. A.; Valent, B.; Jordan, D. B. *Structure* **2001**, *9*, 19.
25. Nakajima, K.; Yamashita, A.; Akama, H.; Nakatsu, T.; Kato, H.; Hashimoto, T.; Oda, J.; Yamada, Y. *Proc. Natl. Acad. Sci. U.S.A.* **1998**, *95*, 4876.
26. Ogata, K.; Umeyama, H. *J. Mol. Graph. Model.* **2000**, *18*, 258.
27. Takeda-Shitaka, M.; Nojima, H.; Takaya, D.; Kanou, K.; Iwadate, M.; Umeyama, H. *Chem. Pharm. Bull.* **2004**, *52*, 643.
28. Iwadate, M.; Ebisawa, K.; Umeyama, H. *Chem-Bio. Informatics J.* **2001**, *1*, 136.
29. Laskowski, R. A.; MacArthur, M. W.; Moss, D. S.; Thornton, J. M. *J. Appl. Cryst.* **1993**, *26*, 283.
30. Price, A. C.; Zhang, Y.-M.; Rock, C. O.; White, S. W. *Biochemistry* **2001**, *40*, 12772.
31. Zhang, Y.-M.; Wu, B.; Zheng, J.; Rock, C. O. *J. Biol. Chem.* **2003**, *278*, 52935.
32. Chen, Z.; Jiang, J. C.; Lin, Z.-G.; Lee, W. R.; Baker, M. E.; Chang, S. H. *Biochemistry* **1993**, *32*, 3342.
33. Taguchi, T.; Ebizuka, Y.; Hopwood, D. A.; Ichinose, K. *Tetrahedron Lett.* **2000**, *41*, 5253.
34. Ozawa, M.; Taguchi, T.; Itoh, T.; Ebizuka, Y.; Booker-Milburn, K. I.; Stephenson, G. R.; Ichinose, K. *Tetrahedron* **2003**, *59*, 8793.
35. Sambrook, J.; Fritsch, E. F.; Maniatis, T. *Molecular Cloning. A Laboratory Manyal*, 2nd ed.; Cold Spring Horbor Laboratory: Cold Spring Horbor, NY, 1986.
36. Kierser, T.; Bibb, M. J.; Buttner, M. J.; Chater, K. F.; Hopwood, D. A. *Practical Streptomyces Genetics*; The John Innes Foundation: Norwich, UK, 2000.
37. Yoneda, T.; Komooka, H.; Umeyama, H. *J. Protein Chem.* **1997**, *16*, 597.
38. Takeda-Shitaka, M.; Umeyama, H. *FEBS Lett.* **1998**, *425*, 448.
39. Takeda-Shitaka, M.; Takaya, D.; Chiba, C.; Tanaka, H.; Umeyama, H. *Curr. Med. Chem.* **2004**, *11*, 551.